CLEO CONF 98-25
ICHEP98 859

Search for $B \to \rho^0 K^0$, $B \to K^{*\pm}\pi^{\mp}$

CLEO Collaboration

(July 21, 1998)

Abstract

We report the results of a search for the decays $B^0 \to \rho^0 K^0$, $B^0 \to K^{*+}\pi^-$, and $B^0 \to K^{*+}K^-$ (and their charge conjugate states). Using 6×10^6 $B\overline{B}$ pairs collected by the CLEO detector at the Cornell Electron Storage Ring, we perform an unbinned maximum likelihood fit to extract signal yields. We set upper limits for all three modes at $\mathcal{B}(B^0 \to \rho^0 K^0) < 3.6 \times 10^{-5}$, $\mathcal{B}(B^0 \to K^{*+}\pi^-) < 4.5 \times 10^{-5}$, and $\mathcal{B}(B^0 \to K^{*+}K^-) < 1.1 \times 10^{-5}$.

J. P. Alexander,[1] R. Baker,[1] C. Bebek,[1] B. E. Berger,[1] K. Berkelman,[1] V. Boisvert,[1] D. G. Cassel,[1] D. S. Crowcroft,[1] M. Dickson,[1] S. von Dombrowski,[1] P. S. Drell,[1] K. M. Ecklund,[1] R. Ehrlich,[1] A. D. Foland,[1] P. Gaidarev,[1] R. S. Galik,[1] L. Gibbons,[1] B. Gittelman,[1] S. W. Gray,[1] D. L. Hartill,[1] B. K. Heltsley,[1] P. I. Hopman,[1] J. Kandaswamy,[1] D. L. Kreinick,[1] T. Lee,[1] Y. Liu,[1] N. B. Mistry,[1] C. R. Ng,[1] E. Nordberg,[1] M. Ogg,[1,*] J. R. Patterson,[1] D. Peterson,[1] D. Riley,[1] A. Soffer,[1] B. Valant-Spaight,[1] A. Warburton,[1] C. Ward,[1] M. Athanas,[2] P. Avery,[2] C. D. Jones,[2] M. Lohner,[2] C. Prescott,[2] A. I. Rubiera,[2] J. Yelton,[2] J. Zheng,[2] G. Brandenburg,[3] R. A. Briere,[3] A. Ershov,[3] Y. S. Gao,[3] D. Y.-J. Kim,[3] R. Wilson,[3] H. Yamamoto,[3] T. E. Browder,[4] Y. Li,[4] J. L. Rodriguez,[4] S. K. Sahu,[4] T. Bergfeld,[5] B. I. Eisenstein,[5] J. Ernst,[5] G. E. Gladding,[5] G. D. Gollin,[5] R. M. Hans,[5] E. Johnson,[5] I. Karliner,[5] M. A. Marsh,[5] M. Palmer,[5] M. Selen,[5] J. J. Thaler,[5] K. W. Edwards,[6] A. Bellerive,[7] R. Janicek,[7] P. M. Patel,[7] A. J. Sadoff,[8] R. Ammar,[9] P. Baringer,[9] A. Bean,[9] D. Besson,[9] D. Coppage,[9] C. Darling,[9] R. Davis,[9] S. Kotov,[9] I. Kravchenko,[9] N. Kwak,[9] L. Zhou,[9] S. Anderson,[10] Y. Kubota,[10] S. J. Lee,[10] R. Mahapatra,[10] J. J. O'Neill,[10] R. Poling,[10] T. Riehle,[10] A. Smith,[10] M. S. Alam,[11] S. B. Athar,[11] Z. Ling,[11] A. H. Mahmood,[11] S. Timm,[11] F. Wappler,[11] A. Anastassov,[12] J. E. Duboscq,[12] K. K. Gan,[12] T. Hart,[12] K. Honscheid,[12] H. Kagan,[12] R. Kass,[12] J. Lee,[12] H. Schwarthoff,[12] A. Wolf,[12] M. M. Zoeller,[12] S. J. Richichi,[13] H. Severini,[13] P. Skubic,[13] A. Undrus,[13] M. Bishai,[14] S. Chen,[14] J. Fast,[14] J. W. Hinson,[14] N. Menon,[14] D. H. Miller,[14] E. I. Shibata,[14] I. P. J. Shipsey,[14] S. Glenn,[15] Y. Kwon,[15,†] A.L. Lyon,[15] S. Roberts,[15] E. H. Thorndike,[15] C. P. Jessop,[16] K. Lingel,[16] H. Marsiske,[16] M. L. Perl,[16] V. Savinov,[16] D. Ugolini,[16] X. Zhou,[16] T. E. Coan,[17] V. Fadeyev,[17] I. Korolkov,[17] Y. Maravin,[17] I. Narsky,[17] R. Stroynowski,[17] J. Ye,[17] T. Wlodek,[17] M. Artuso,[18] E. Dambasuren,[18] S. Kopp,[18] G. C. Moneti,[18] R. Mountain,[18] S. Schuh,[18] T. Skwarnicki,[18] S. Stone,[18] A. Titov,[18] G. Viehhauser,[18] J.C. Wang,[18] J. Bartelt,[19] S. E. Csorna,[19] K. W. McLean,[19] S. Marka,[19] Z. Xu,[19] R. Godang,[20] K. Kinoshita,[20] I. C. Lai,[20] P. Pomianowski,[20] S. Schrenk,[20] G. Bonvicini,[21] D. Cinabro,[21] R. Greene,[21] L. P. Perera,[21] G. J. Zhou,[21] S. Chan,[22] G. Eigen,[22] E. Lipeles,[22] J. S. Miller,[22] M. Schmidtler,[22] A. Shapiro,[22] W. M. Sun,[22] J. Urheim,[22] A. J. Weinstein,[22] F. Würthwein,[22] D. E. Jaffe,[23] G. Masek,[23] H. P. Paar,[23] E. M. Potter,[23] S. Prell,[23] V. Sharma,[23] D. M. Asner,[24] J. Gronberg,[24] T. S. Hill,[24] D. J. Lange,[24] R. J. Morrison,[24] T. K. Nelson,[24] D. Roberts,[24] B. H. Behrens,[25] W. T. Ford,[25] A. Gritsan,[25] H. Krieg,[25] J. Roy,[25] and J. G. Smith[25]

[1]Cornell University, Ithaca, New York 14853
[2]University of Florida, Gainesville, Florida 32611
[3]Harvard University, Cambridge, Massachusetts 02138
[4]University of Hawaii at Manoa, Honolulu, Hawaii 96822
[5]University of Illinois, Urbana-Champaign, Illinois 61801
[6]Carleton University, Ottawa, Ontario, Canada K1S 5B6

[*]Permanent address: University of Texas, Austin TX 78712.

[†]Permanent address: Yonsei University, Seoul 120-749, Korea.

and the Institute of Particle Physics, Canada
[7]McGill University, Montréal, Québec, Canada H3A 2T8
and the Institute of Particle Physics, Canada
[8]Ithaca College, Ithaca, New York 14850
[9]University of Kansas, Lawrence, Kansas 66045
[10]University of Minnesota, Minneapolis, Minnesota 55455
[11]State University of New York at Albany, Albany, New York 12222
[12]Ohio State University, Columbus, Ohio 43210
[13]University of Oklahoma, Norman, Oklahoma 73019
[14]Purdue University, West Lafayette, Indiana 47907
[15]University of Rochester, Rochester, New York 14627
[16]Stanford Linear Accelerator Center, Stanford University, Stanford, California 94309
[17]Southern Methodist University, Dallas, Texas 75275
[18]Syracuse University, Syracuse, New York 13244
[19]Vanderbilt University, Nashville, Tennessee 37235
[20]Virginia Polytechnic Institute and State University, Blacksburg, Virginia 24061
[21]Wayne State University, Detroit, Michigan 48202
[22]California Institute of Technology, Pasadena, California 91125
[23]University of California, San Diego, La Jolla, California 92093
[24]University of California, Santa Barbara, California 93106
[25]University of Colorado, Boulder, Colorado 80309-0390

I. INTRODUCTION

Two-body decays of B mesons into final states containing a π or K and a ρ or K^* are the pseudoscalar-vector analogs of the two-pseudoscalar modes $B \to K\pi/\pi\pi/KK$ that have received much attention in recent years. In $B \to K\pi/\pi\pi/KK$, CLEO has observed three of the four possible $B \to K\pi$ decay modes and none of the $\pi\pi$ or KK final states, despite comparable sensitivity for all three processes. These findings suggest that gluonic $b \to s$ penguin transitions (Figure 1(b)) are the dominant physics processes in charmless hadronic B decays to two pseudoscalar mesons.

Since $\rho^0 K_S^0$ is a CP eigenstate, it may be possible to measure time-dependent CP asymmetries with this mode. The weak phase in $B \to \rho^0 K_S^0$ is approximately equal to that in $B \to J/\psi K_S^0$. Thus, both modes can be used to probe the angle β of the unitarity triangle [1]. However, new physics phenomena will, in general, affect these two modes differently because they are dominated by different orders of the weak coupling. Therefore, comparing future measurements of β using these two decay modes is of particular interest.

The decay $B^0 \to K^{*+}\pi^-$ may be used to study direct CP violation. Since the rate for $B^0 \to K^{*+}K^-$ is predicted to be much smaller than that for $B^0 \to K^{*+}\pi^-$, the final state where $K^{*+} \to \pi^+ K_S^0$ does not suffer appreciably from the K/π ambiguity that plagues many other attempts to measure direct CP violation in B decays. Also, upper limits on modes like $B^0 \to K^{*+}K^-$ will be important in establishing the amount of final state rescattering, essential for interpreting measurements of the angle γ of the unitarity triangle [2].

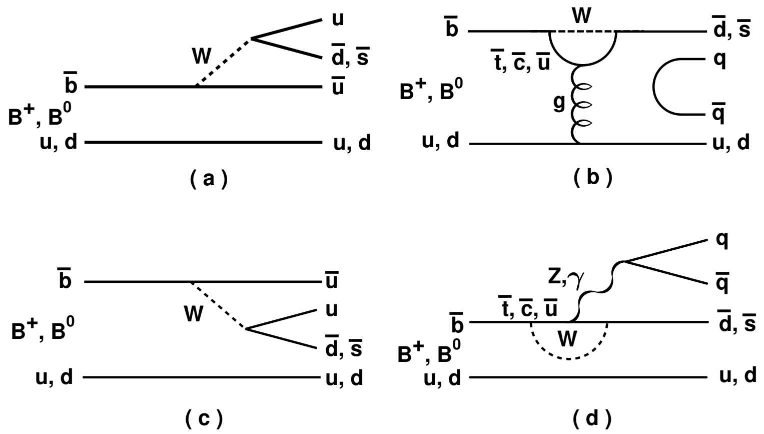

FIG. 1. The dominant Feynman diagrams contributing to pseudoscalar-vector decays of a B meson: (a) external W-emission, (b) gluonic penguin, (c) internal W-emission, and (d) external electroweak penguin. Vertical penguins and W-exchange diagrams have been neglected.

II. EVENT AND CANDIDATE SELECTION

The data sample used in this analysis was produced in symmetric e^+e^- collisions at the Cornell Electron Storage Ring and collected by the CLEO II and CLEO II.V detectors. It comprises 5.59 fb^{-1} collected on the $\Upsilon(4S)$ resonance, corresponding to 6 million $B\overline{B}$ pairs, of which 2.5 million were taken with CLEO II.V. An additional 2.87 fb^{-1} collected slightly below the $B\overline{B}$ production threshold is used for background studies.

In CLEO II, described in detail in [3], the momenta of charged particles are measured with a tracking system consisting of a 6-layer straw tube chamber, a 10-layer precision drift chamber, and a 51-layer main drift chamber, all operating inside a 1.5 T superconducting solenoid. The main drift chamber also provides a measurement of the specific ionization loss, dE/dx, which is used for particle identification. For CLEO II.V the 6-layer straw tube chamber was replaced by a 3-layer double sided silicon vertex detector, and the gas in the main drift chamber was changed from an argon-ethane to a helium-propane mixture. Photons are detected with a 7800-crystal CsI electromagnetic calorimeter, which is also inside the magnet. Muons are identified using proportional chambers placed at various depths within the steel return yoke of the magnet.

Charged tracks are required to be well-measured and to pass track quality requirements based on the average hit residual and the impact parameters in both the $r-\phi$ and $r-z$ planes. In addition, tracks that are consistent with being electrons or muons are not allowed to form the B candidate.

K^0_S candidates are selected from pairs of tracks with invariant mass within 10 MeV/c^2, approximately 2.5 standard deviations (σ), of the nominal K^0_S mass. In addition, K^0_S candidates are required to originate from the beam spot and to have well-measured displaced decay vertices.

We form ρ^0 candidates from $\pi^+\pi^-$ pairs with invariant mass within 450 MeV of the nominal ρ^0 mass. K^{*+} candidates are selected from $K^0_S\pi^+$ combinations with invariant mass within 200 MeV of the nominal K^{*+} mass.

A. Kinematic Constraints

We form neutral B candidates by combining two charged tracks and a K^0_S candidate that pass the cuts described above. Instead of calculating the invariant mass of the B candidate, we use our knowledge of its energy, which is equal to the the beam energy (E_{beam}) to form a beam-constrained mass, $m_B \equiv \sqrt{E^2_{\mathrm{beam}} - |\sum_i \mathbf{p}_i|^2}$, where the $\mathbf{p}_i$ are the momenta of the B candidate's daughters. The beam constraint improves the resolution of m_B by an order of magnitude to about 3 MeV for the modes considered in this paper. The beam-constrained mass for all B candidates is required to lie between 5.2 and 5.3 GeV. While the beam-constrained mass is an expression of momentum conservation, we also exploit energy conservation by calculating $\Delta E \equiv \sum_i E_i - E_{\mathrm{beam}}$, where the E_i are the energies of the B candidate's daughters. For the topology of our signal decays, the ΔE resolution is roughly 20 MeV for CLEO II. CLEO II.V benefits from improved momentum resolution, which results in a ΔE resolution that is 20% narrower. For this analysis, we accept only candidates with $|\Delta E|$ less than 200 MeV.

Using this sample of B candidates, we search for the decays $B \to \rho^0 K^0$ and $B \to K^{*+}h^-$ with $K^{*+} \to K^0\pi^+$, where h^- denotes a charged kaon or pion. We only consider final states with $K^0_S \to \pi^+\pi^-$. Charge conjugate states are implied throughout. For the $K^{*+}h^-$ modes, ΔE is calculated assuming the h^- to be a pion. The ΔE distribution for $\rho^0 K^0$ and $K^{*+}\pi^-$

is centered at zero, while that for $K^{*+}K^-$ is centered at -42 MeV.

B. Helicity Angle

Decays of a pseudoscalar to another pseudoscalar and a vector can be characterized by the helicity angle, which is defined (for two-body decays of the vector) to be the angle between the direction of a daughter track in the vector's rest frame and the direction of the vector in the B candidate's rest frame. Helicity conservation dictates that the polarization of the vector meson is purely transverse. Therefore, the helicity angle for signal exhibits a $\cos^2\theta$ dependence while the background is more or less flat in $\cos\theta$. This $\cos^2\theta$ distribution implies that the daughters of the vector tend to emerge along the parent's flight direction (in the lab). Consequently, the momentum spectrum of the daughters is bimodal; one daughter has high momentum, and the other has low momentum.

The helicity angle distribution is a powerful discriminator between signal and background, which can be used to full effect in the maximum likelihood fit, which is described below. However, the signal shape is not strictly a $\cos^2\theta$ distribution. Rather, the distribution falls off at the edges because of limited tracking efficiency for particles with momenta below 200 MeV. Also, the shapes for both signal and background are distorted by the combinatoric background, which preferentially populates the low-momentum region. To be less sensitive to these effects, we require $|\cos\theta_{hel}| < 0.9$ for the $\rho^0 K^0_S$ mode and $\cos\theta_{hel} > -0.86$ for the $K^{*+}h^-$ modes, where the K^* helicity angle is measured using the flight direction of the daughter pion.

C. D Veto

A significant portion of the background from other B decays is caused by the decay $B^0 \to D^-\pi^+$, with $D^- \to K^0_S\pi^-$. Therefore, we reject candidates where the invariant mass of the K^0_S with either of the two pions lies within 3σ (~ 20 MeV) of the nominal D mass. This veto is placed in the $B^0 \to \rho^0 K^0_S$ analysis only, as it was found to be unnecessary in the $B^0 \to K^{*+}h^-$ modes due to the narrower width of the K^{*+}. The residual cross-feed from $B^0 \to D^-\pi^+$ as well as from other $B \to D$ modes is 0.3 events for $B^0 \to \rho^0 K^0_S$ and 0.02 events for $B^0 \to K^{*+}\pi^-$. These contributions are subtracted from the signal yield returned from the maximum likelihood fit.

III. EVENT TOPOLOGY FOR BACKGROUND SUPPRESSION

The $\Upsilon(4S)$ resonance sits atop a background of $e^+e^- \to q\overline{q}$, where $q = u, d, s, c$, which has a cross section approximately three times larger than for $e^+e^- \to \Upsilon(4S) \to B\overline{B}$. To help suppress this continuum background, we make use of the sphericity angle, θ_{sph}, which is the angle between the sphericity axes of the B candidate and of the rest of the event. The $\cos\theta_{sph}$ distribution peaks strongly at ± 1 for continuum background events and is nearly flat for signal. For the analysis presented here, 83% of the continuum background is eliminated by requiring $|\cos\theta_{sph}|$ to be less than 0.8.

Additional separation of signal from $q\overline{q}$ background is provided by a Fisher discriminant, which is described in detail in Ref. [4]. The Fisher discriminant is a linear combination of eleven variables, x_i:

$$\mathcal{F} \equiv \sum_{i=1}^{11} \alpha_i x_i.$$

These eleven variables are $\cos\theta_{cand}$ (θ_{cand} is the angle between the sphericity axis of the candidate and the beam axis), R_2 (the ratio of the Fox-Wolfram moments H_2/H_0 [5]), and the sums of momentum magnitudes in nine concentric 10° cones around the candidate thrust axis. The coefficients α_i are chosen to maximize the separation between signal and background Monte Carlo samples. For the event topology considered in this analysis, the Fisher discriminant provides approximately 1σ statistical separation between signal and continuum background.

IV. MAXIMUM LIKELIHOOD FIT

An unbinned maximum likelihood fit is used to extract signal yields from the candidates passing the selection cuts described above. The likelihood of the sample is defined to be the product of the individual likelihoods for each event. For a single event, the likelihood is a sum over fit hypotheses of the probability for that event to contribute to each hypothesis:

$$\mathcal{L} = \prod_{j}^{\#entries} \left(\sum_{i}^{\#hypotheses} P_j^i f_i \right).$$

P_i^j is the joint probability for event j under the hypothesis i and is a function of all the input variables.

The free parameters to be varied in the fit are the yield fractions f_i of each hypothesis. For $\rho^0 K_S^0$, there are only two hypotheses: signal and background. Furthermore, the two fractions are constrained to sum to unity, so there is only one free parameter in this fit. The two $K^{*+}h^-$ modes are fit simultaneously, using dE/dx and ΔE to resolve the K/π ambiguity. This fit includes four hypotheses (signal/background, $h = \pi/K$), and hence, three degrees of freedom. The likelihood can therefore be interpreted as the total probability for the input sample to contain the corresponding yield fractions f_i.

For each event in the data sample, the following information is input to the fit:

- The beam-constrained mass, m_B.
- ΔE.
- The Fisher discriminant, $\mathcal{F}$.
- $\cos\theta_B$, where θ_B is the angle between the flight direction of the reconstructed B and the beam axis. For real B mesons this variable exhibits a $\sin^2\theta$ dependence. The flight direction of misreconstructed B candidates is randomly distributed, so $\cos\theta_B$ is flat for background.
- The intermediate resonance masses, m_ρ and m_{K^*}.

- $\cos\theta_{hel}$.

Thus, for example, the signal probability for a given event in the $\rho^0 K_S^0$ fit is:

$$P_i^{sig} = P_{m_B}^{sig}(m_{B_i}) P_{\Delta E}^{sig}(\Delta E_i) P_{\mathcal{F}}^{sig}(\mathcal{F}_i) P_{\cos\theta_B}^{sig}(\cos\theta_{B_i}) P_{m_\rho}^{sig}(m_{\rho_i}) P_{\cos\theta_{hel}}^{sig}(\cos\theta_{hel_i}),$$

In the $K^{*+}h^-$ fit, additional use is made of the dE/dx of the bachelor track, h^-, to help identify it as a π^- or a K^-.

The signal PDFs are obtained from a GEANT-based Monte Carlo [6] and the background PDFs from a combination of off-resonance data and the on-resonance sideband ($m_B < 5.27$ GeV). The on-resonance data is not included in the measurement of the background m_B shape. The same PDF parameters are used for CLEO II and CLEO II.V except for signal ΔE and dE/dx variables because both of these have improved resolution in CLEO II.V. All PDFs are normalized to unit area over the fiducial region.

In addition to the signal yields returned from the fit, we can also calculate the 90% confidence level yield upper limits, N^{90}, which are defined by

$$\frac{\int_0^{N^{90}} \mathcal{L}_{max}(N)dN}{\int_0^{\infty} \mathcal{L}_{max}(N)dN} = 0.90, \tag{1}$$

where $\mathcal{L}_{max}(N)$ is the optimal likelihood at fixed N. This method of calculating the upper limit conservatively accounts for possible correlations among the free parameters in the fit.

V. SYSTEMATIC ERRORS

Systematic errors on the fitted yields are evaluated by introducing random Gaussian-distributed variations of the PDF parameters while accounting for the important correlations between these parameters. For each variation, the data is refit, and the spread in yield for an ensemble of such fits provides an estimate of the systematic error. For all background distributions, the widths of the parameter variations are the uncertainties from the measurements of the PDF parameters. For the signal PDFs, where the parameters are determined from Monte Carlo, the sizes of the Gaussian variations are set at values determined from independent data samples.

Systematically degraded upper limits for the signal yield are obtained by summing the likelihood as a function of the yield for all the trials in the ensemble. This curve is then integrated to 90% of its area, as described in Equation 1. Branching fraction upper limits are calculated using detection efficiencies reduced by their systematic errors.

VI. RESULTS

The CLEO II and CLEO II.V data sets are fitted simultaneously, and the resultant background-subtracted signal yield upper limits, as well as the branching fraction upper limits (including systematic errors) are given in Table I. For comparison, we also include a range of theoretical predictions [7–9].

TABLE I. Background-subtracted fitted signal yield upper limits with systematic errors and the corresponding branching fraction upper limits. All upper limits reflect a 90% confidence level. Also included are the detection efficiencies (reduced by their systematic error) and a range of theoretical predictions for the branching fractions of these modes. Both the branching fraction upper limits and the theoretical predictions are given in units of 10^{-5}.

Mode	N_{sig} UL	$\mathcal{E}(\%)$	$\mathcal{B}$ UL	Theory [7–9]
$\rho^0 K_S^0$	< 19.7	9.5	< 3.6	$0.04 - 2$
$K^{*+}\pi^-$	< 17.0	6.5	< 4.5	$0.6 - 8$
$K^{*+}K^-$	< 4.2	6.4	< 1.1	~ 0.001

As an illustration of these results, Figure 2 shows m_B and ΔE projections for the three modes. To reduce the background entering these plots, tight cuts are placed on all input variables except the one plotted. The overlaid curves are the PDFs used in the fit, normalized to the signal yield upper limit or to the background yield and scaled by the efficiency of the additional cuts. We show both the sum of the signal and background PDFs as well as the background PDFs alone.

VII. SUMMARY AND CONCLUSIONS

We have searched for rare two-body hadronic B decays to a pseudoscalar and a vector meson where the final state consists of two charged tracks and a K_S^0. An unbinned maximum likelihood fit yields branching fraction upper limits of $\mathcal{B}(B^0 \to \rho^0 K^0) < 3.6 \times 10^{-5}$, $\mathcal{B}(B^0 \to K^{*+}\pi^-) < 4.5 \times 10^{-5}$, and $\mathcal{B}(B^0 \to K^{*+}K^-) < 1.1 \times 10^{-5}$. These upper limits are at least an order of magnitude higher than the bulk of the theoretical predictions for these modes.

ACKNOWLEDGMENTS

We gratefully acknowledge the effort of the CESR staff in providing us with excellent luminosity and running conditions. J.R. Patterson, and I.P.J. Shipsey thank the NYI program of the NSF, M. Selen thanks the PFF program of the NSF, M. Selen and H. Yamamoto thank the OJI program of DOE, J.R. Patterson, K. Honscheid, M. Selen and V. Sharma thank the A.P. Sloan Foundation, M. Selen thanks Research Corporation, S. von Dombrowski thanks the Swiss National Science Foundation, and H. Schwarthoff thanks the Alexander von Humboldt Stiftung for support. This work was supported by the National Science Foundation, the U.S. Department of Energy, and the Natural Sciences and Engineering Research Council of Canada.

REFERENCES

[1] Unitarity of the CKM matrix implies $V_{ud}V_{ub}^* + V_{cd}V_{cb}^* + V_{td}V_{tb}^* = 0$, which describes a triangle in the complex plane. The angles of this triangle are denoted by $\beta = -\mathrm{Arg}(V_{td})$, $\gamma = \mathrm{Arg}(V_{ub}^*)$, and $\alpha = \pi - \beta - \gamma$ in the Wolfenstein parametrization, L. Wolfenstein, Phys. Rev. Lett. **51**, 1945 (1983).

[2] M. Gronau and J. Rosner, EFI-98-23(1998), hep-ph/9806348.

[3] Y. Kubota *et al.* (CLEO Collaboration), Nucl. Instr. Methods Phys. Res. A**320**, 66 (1992).

[4] D.M. Asner *et al.* (CLEO Collaboration), Phys. Rev. D **53**, 1039 (1996).

[5] G. Fox and S. Wolfram, Phys. Rev. Lett. **41**, 1581 (1978).

[6] R. Brun *et al.*, CERN DD/EE/84-1.

[7] A. Ali, G. Kramer, Cai-Dian Lü, hep-ph/9804363.

[8] M. Ciuchini *et al.*, hep-ph/9708222.

[9] L.-L. Chau *et al.*, Phys. Rev. D **43**, 2176 (1991).

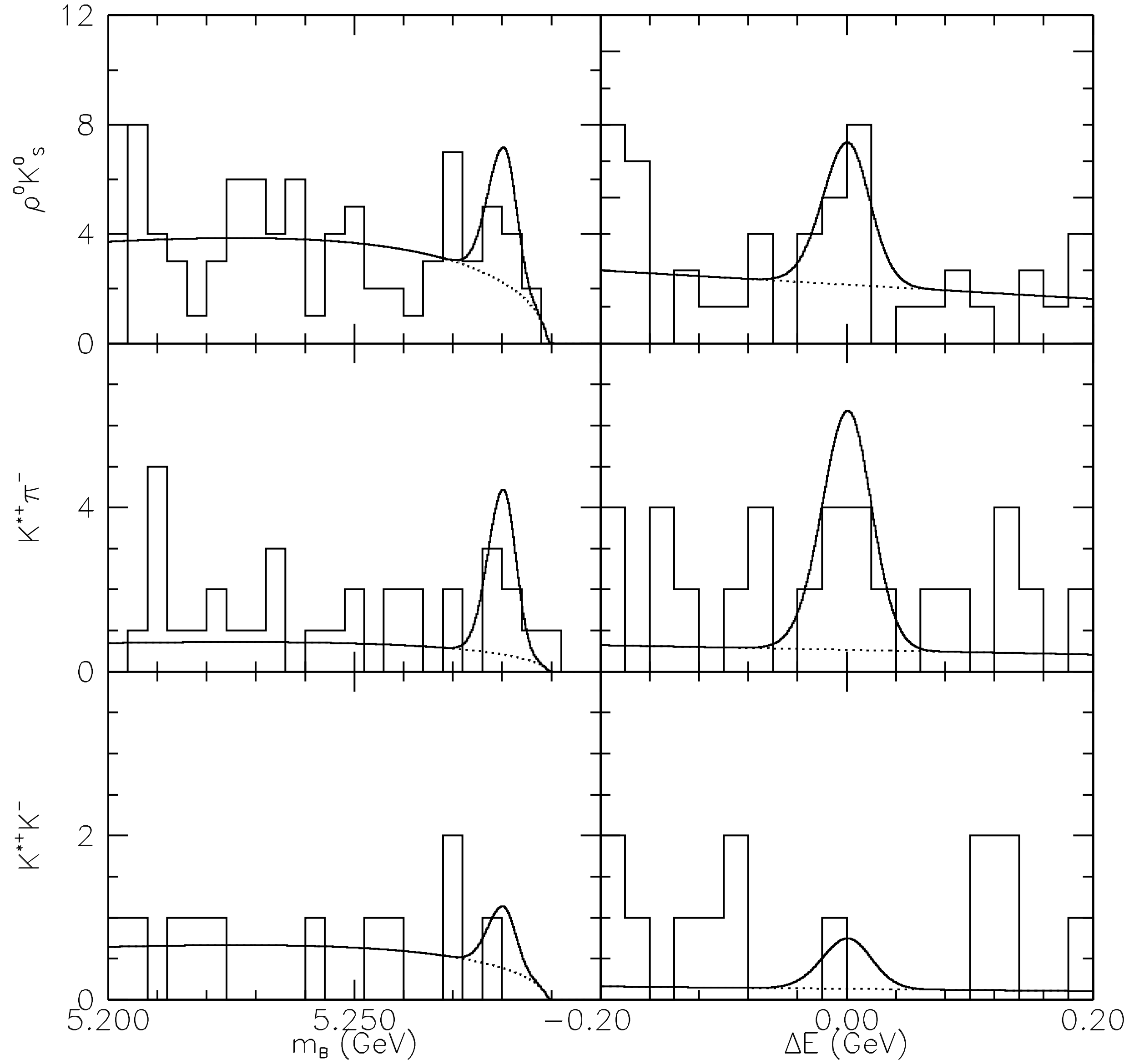

FIG. 2. m_B and ΔE projections for $B^0 \to \rho^0 K^0_S$ (top), $B^0 \to K^{*+}\pi^-$ (middle), and $B^0 \to K^{*+}K^-$ (bottom). The dotted curves are the scaled projections of the background yield reported by the fit. The solid curves include the scaled projections of the signal yield upper limits, *not* of the yield itself, as reported by the fit.